Statistical analysis of the likelihood of bars in disk galaxies

Author: Josep Canadell Juanals.
Facultat de Física, Universitat de Barcelona, Diagonal 645, 08028 Barcelona, Spain.

Advisor: José Maria Solanes Majua

Abstract: We make use of HI content information from the Arecibo Legacy Fast ALFA survey catalog to study the stellar and atomic gas content of barred disk galaxies. These 21-cm observations are augmented with the extensive optical data gathered in the NASA-Sloan Atlas catalog and with information on galaxy morphologies and bar probabilites included in the catalog by Domínguez Sánchez et al. (2018). We find, in agreement with previous studies, that the bar probability of the disk population shows a bimodal distribution, both in terms of the stellar mass and the $(g-r)$ optical color, which we attribute to the tendency of the late disks to be low-mass, blue objects, while earlier spirals are more massive and redder. We also confirm that the bar fraction decreases with increasing gas mass fraction and neutral hydrogen excess. This anticorrelation results from the inhibiting effect the gas has in the formation of bars.

I. INTRODUCTION

Stellar bars are an important component of many disk galaxies. They are believed to be key drivers of they secular evolution, in part because they can act as both sources and sinks for angular momentum, re-distributing stars, gas, and dark matter within galaxies [4]. The most visible aspect of this is bar-driven gas inflow and subsequent star formation in the central regions of galaxies, which has been suggested to play a key role in building up bulges. Bars also have long been suspected to participate in the fueling of AGN [2].

Likewise, the mere presence or absence of bars can provide important insights into galactic evolution. The discovery from early simulations that N-body disks systematically became bar-unstable raised the question of why some disk galaxies did not have bars. The demonstration in the pioneering work by [3] that massive halos could stabilize disks against bar formation was one of the reasons that led to the acceptance of dark-matter halos. On the other hand, the appearance of bars in galaxies can be a useful and easily visible indicator of when and how rapidly disks become kinematically cool [5].

Observational studies have shown that bars are more frequent in massive, red galaxies with early-type morphologies [14], highlighting that the formation of bars is strongly dependent on the physical properties of the hosting galaxy. One crucial component in the formation process and evolution of bars is the gas fraction in the galaxy. When a galaxy is rich in gas, a significant exchange of angular momentum is expected to occur between the stellar and gas components [1], increasing the rotation frequency of the bar, weakening it and, ultimately, destroying it. The adverse effects of gas on the evolution of the bar could explain why the bar fraction observed in local galaxies decreases for increasing gas mass fraction [13].

In this work we study the dependence of the bar fraction on the gas mass ratio and other galaxian properties with the aim of disentangling if the decrease on the bar fraction of gas-rich galaxies is caused by bars promoting the consumption of gas and/or if the increase of gas content inhibits bar formation. The data used are presented in Section II. The main results and discussion are presented in Section IV. Lastly, we summarize our general conclusions in Section V. Throughout this paper, we use a standard flat cosmology with density parameter $\Omega_{\rm m} = 0.3$, cosmological constant $\Omega_\Lambda = 0.7$ and Hubble constant $H_0 = 100h$ km s^{-1} Mpc^{-1}, with $h = 1$.

II. DATA

The data used in the present analysis are taken from different public sources. We rely on two large galaxy catalogs compiled from large-scale blind surveys: the UV/optical/NIR observations given in the NASA-Sloan Atlas (NSA) spectroscopic catalog, v1.0.1, and the recently finished 21-cm Arecibo Legacy Fast ALFA Survey (ALFALFA; [16]) catalog of extragalactic sources of neutral hydrogen (HI). The first dataset is selected to include virtually all galaxies with known redshifts out to about $z < 0.15$ within the coverage of the Main Galaxy Sample of the Sloan Legacy Survey [6]. The SDSS optical/NIR detections are completed with data from other surveys, including the ultraviolet Galaxy Evolution Explorer survey (GALEX; [17]). For the much more shallower ALFALFA survey ($cz_{\rm max} \simeq 18,000$ km s^{-1}), we use data from its final data release $\alpha.100$ which covers the totality of the survey area [7]. The original data of these catalogs have been augmented with information from other sources, the most important being the automated galaxy morphologies and bar probabilities listed in the catalog recently published by [15].

The final datasets contain data for about 633,000 and 31,000 galaxies, respectively. The Sloan-based catalog has 51 different entries, while the ALFALFA-based catalog contains a total of 69, including informations on the total mass of HI, the ratio between HI mass and the stellar mass and an estimate of the HI deficiency.

III. DATA TREATMENT

A. Morphological classification and bar fractions

Galaxy morphologies and bar probabilities are retrieved from the catalog by [15] that lists these informations for $\sim 671,000$ Sloan galaxies. The classification of such a huge number of objects is obtained thanks to Deep Learning algorithms that use Convolutional Neural Networks trained with color images from both the Galaxy Zoo 2 [8] and the visual classification catalog of[14]. We adopt the data based on the comparison with the latter dataset. Morphological classifications are provided in terms of the numerical T-type (T) parameter (see [9] and references therein). The average scatter of this automated classification is only $\sigma = 1.1$, so the accuracy is comparable or even better than that of expert classifier intercomparisons. In addition, [15] provide the probability of being S0 ($P_{\rm S0}$) which, for objects with $T \leq 0$, efficiently allows distinguishing between pure E and S0 galaxies. In the present work, and according to these authors, we consider S0 any object with $T \leq 0$ and $P_{\rm S0} > 0.8$. Such a conservative value for the probability has been chosen to try to prioritize the purity of the S0 sample while preserving a sufficient number of objects for the analysis. Finally, we consider barred galaxies those objects with a probability of having a bar, P_{bar}, according to the Nair & Abraham criteria larger than 0.5.

B. Selection of volume-limited samples

To avoid selection biases arising from the preferential detection of intrinsically bright objects it will be necessary on certain occasions to deal with subsamples of the main datasets in which a minimum value of an intrinsic property can be detected for all objects within a given cosmic volume. As such, these subsets of data should be free of the Malmquist bias. Given that both the NSA and ALFALFA catalogs are essentially complete up a given flux threshold[19], volume-limited samples can be easily obtained by cutting off the data at the edge where the objects with the lowest value of the intrinsic property would be hitting the limiting flux.

It is well known that the Sloan Legacy data are essentially complete for extended objects with extinction corrected Petrosian r-magnitudes below $m_{\rm lim} = 17.7$. Thus, for the NSA catalog, we have chosen to select a limiting absolute Petrosian magnitude in the r-band $M_r < 20.0$, as this threshold has the characteristic of maximizing the number of objects that can be included in a volume-limited subset of this dataset. From the magnitude equation:

$$M_r = m_r - 25 - 5\log_{10} D, \qquad (1)$$

where M_r and m_r are, respectively the r-band absolute and apparent magnitudes, and D is the cosmic luminosity distance, one gets that the maximum distance of such subset is $d_{\rm max} = 316.23$ Mpc. We also introduce a lower limit in the data of 30 Mpc to exclude those (few) galaxies with most uncertain measurements due to their closeness or large apparent brightness.

In Figure (1) we provide a plot of distance (horizontal axis) versus absolute magnitude (vertical axis) for the NSA-based data. In this plot, called a Spanhauer diagram, we show the different limitations applied in the definitions of our complete and volume-limited datasets. Note the top and bottom blue curves, which are additional restrictions corresponding to limits in the apparent magnitude between $m_r = -25$ and $m_r = 11.5$, respectively. Galaxies outside this range of fluxes are excluded because we suspect that they correspond to objects with highly implausible measurements.

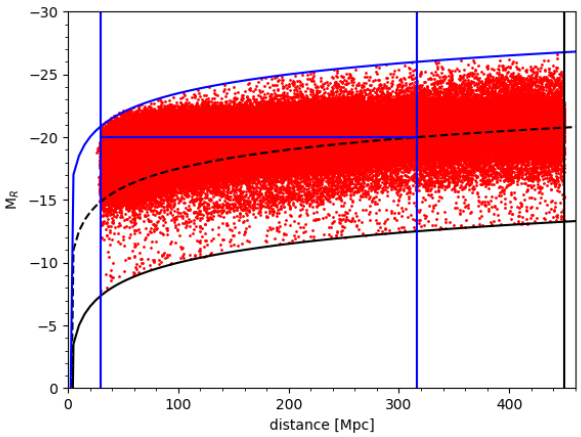

FIG. 1: Scattered plot of the M_r versus the distance of the NSA galaxies. The galaxies enclosed by the blue lines are the ones with volume-limited conditions.

Likewise, we are interested in defining a subset of the ALFALFA catalog which is complete in HI mass (see next Section). HI masses are estimated using the formula by [10]

$$\frac{M_{\rm HI}}{M_\odot} = 2.356 \times 10^5 \frac{D}{\rm Mpc} \frac{S_{21}}{\rm Jy\ km\ s^{-1}} \qquad (2)$$

where S_{21} is the integrated HI line flux density. For this catalog, the integrated flux limit that guarantees a reasonable completeness is, according to [18], $S_{21} = 1.3$ Jy km s^1. As in the case of the NSA catalog, we have explored different values of the HI mass trying to maximize the number of objects included in the volume limited sample and, simultaneously, guaranteeing a large enough dynamic range for this variable. Finally, we choose to adopt the volume-limited sample defined by the HI mass threshold $\log_{10} M_{\rm HI} > 9.25 M_\odot$, which according to equation (2) corresponds to a maximum distance of 76.19 Mpc and encompasses 3,349 galaxies. Figure (2) illustrates

the limits adopted in the definition of both the complete and volume-limited ALFALFA-based datasets. As with the NSA data, we introduce a lower limit of 30 Mpc to exclude the galaxies with most uncertain distances

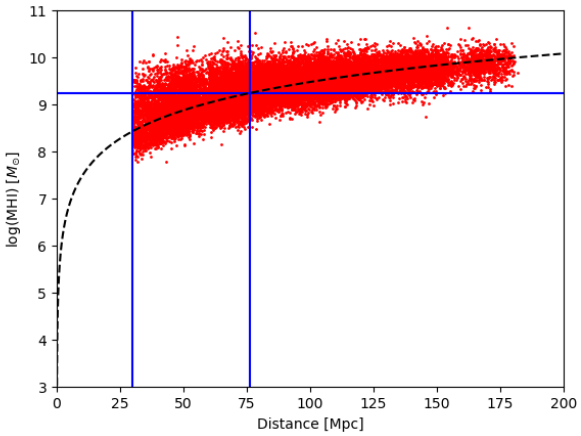

FIG. 2: Scattered plot of the $M_{\rm HI}$ versus the distance of the ALFALFA galaxies

C. Statistics of bar fractions

Whenever it is possible we split of our data into four Hubbles subtypes: S0, Sa, Sb, and Sc. As mentioned earlier, the S0 galaxies are those with $T \leq 0$ and $P_{\rm S0} > 0.8$. The Sa galaxies have rounded T-types between 1 and 2, the Sb between 3 and 4, and the Sc between 5 and 6. The few later objects with T-types greater than 6.5 are not studied separately, but are taken into account when calculating the bar fraction for the entire population of disk galaxies (labelled in all plots All S). The bar frequency behaves in an ordered fashion with morphology, with later types showing higher bar fractions than earlier objects, so F_{bar}(Sc)> F_{bar}(Sb)> F_{bar}(Sa)> F_{bar}(S0) (see the Figs. of the next Section).

Each property under investigation is divided into several bin (usually between 7 and 10), and the fraction of barred systems per bin is calculated from the ratio N_{bar}/N_{tot} that compares the number of galaxies with a bar with the total number galaxies in that bin. The uncertainties on these fractions are computed assuming binomial statistics: $\sigma = \sqrt{N_{\rm bar}}/N_{\rm tot}$. For the sake of clarity, we have excluded from the plots bins with a small total number of galaxies (usually $N_{tot} < 10$).

IV. RESULTS AND DISCUSSION

Our analysis is focused on the dependence of the bar fraction with the stellar mass, the optical color, the HI mass fraction, and the excess of HI gas.

A. Stellar Mass $\log M_*$

The parameter $\log M_*$ is used to represent stellar mass in units relative to the mass of our Sun.

As this magnitude can be affected by Malmquist bias, the calculation of bar fractions demands a volume-limited dataset. This limitation, however, is not as dramatic as in the case of 21-cm observations (see Secs. IV.C and IV.D below) since it is applied on the NSA-based catalog, which initially contains 376,877 galaxies with M_* measurements, of which 34,922 present a bar. Imposing the volume-limited condition still leaves a subset with 112,217 galaxies, of which 16,127 are barred, which allows us to improve on sample size by over an order of magnitude compared to previous studies, as well as extend our investigation to the main subtypes of disk galaxies. The

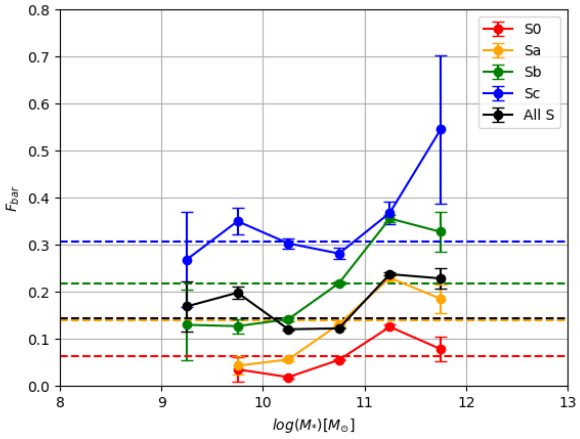

FIG. 3: Relation between the bar fraction and the logarithm of the stellar mass, for the S0 (red), Sa (yellow), Sb (green), Sc (blue) and all the types together (black). The discontinuous lines are the average value.

Figure (3) depicts the fraction of barred systems in each mass bin for our sample of disk objects. It clearly shows that while the bar fraction of the different types of disk increases roughly monotonically with increasing stellar mass, the bar fraction of the whole spiral population exhibits a bimodal behavior. The latter result is in good agreement with the findings of [14]. However, contrarily to these authors, we do not believe that this bimodality bears a physical connection with the mass associated with the transition from the blue cloud to the red sequence [11]. Instead, we attribute it simply to the fact that late-type galaxies clearly prefer the low-mass peak, while early-type galaxies prefer the high-mass peak.

B. Optical color $(g - r)$

Optical color is represented by the difference between the absolute magnitudes in the g and r SDSS windows.

In this case we use again the NSA-based catalog which allows us to work with a superb statistics. We find results that are consistent with those of the previous section because stellar mass and color are two properties that show a good correlation. As illustrated in the Figure (4), the behavior of the general disk population (black curve) is also bimodal. As for the stellar mass, this happens because the different subtypes of spirals are segregated in color. The fact that the blue mode is dominated basically by the Sc and the earlier types contribute mostly to the red mode and the bar fraction decreases towards the earliest types explains why the blue peak is higher than the red one.

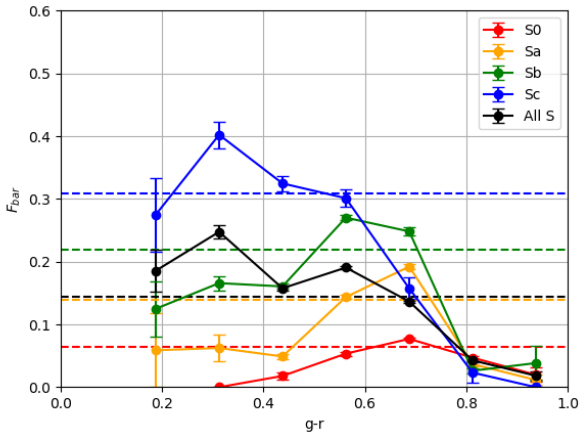

FIG. 4: Relation between the bar fraction and the color (g-r), for the S0 (red), Sa (yellow), Sb (green), Sc (blue) and all the types together (black). The discontinuous lines are the average value.

However, our result (and that of [14]) is markedly different from the finding of [13] that their disk bar fraction increased almost monotonically towards redder colors. We suspect that this different behavior is due to the fact that the Masters dataset was biased against low-mass blue disks, an argument which is supported by their observation of a higher bar fraction in disk galaxies with higher stellar mass.

C. HI mass fraction $f_{\rm HI}$

This property is defined as the decimal logarithm of the ratio $M_{\rm HI}/M_*$.

In this case the number of data available is rather small because not all ALFALFA galaxies have information on M_*. The cross-match between the 21-cm data and the NSA measurements results in a dataset with a total of 506 galaxies of which 117 show a bar. Fortunately, it is not necessary to reduce further the sample size by working with a volume-limited sample since the HI mass fraction is a distance-independent quantity. However, the limited number of objects prevent us from studying the behavior of the S0 separately, though they are taken into account when calculating the bar fraction for the entire population of disks.

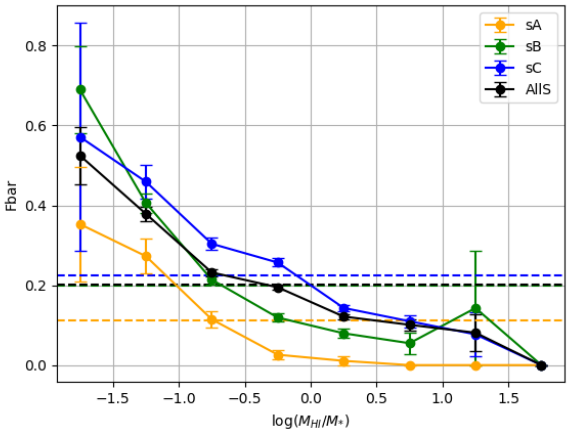

FIG. 5: Representation of the bar fraction vs the $\log(M_{\rm HI}/M_*)$ for the Sa (yellow), Sb (green), Sc (blue) and all the galaxy types (black). The discontinuous lines are the average value

Consistently with former studies ([13]) we see in Figure (5) that the presence of bars decreases as the ratio between the $M_{\rm HI}$ and M increases. Our larger statistics also allows us to observe that the decrement is essentially monotonic and that all Hubble types behave similarly. Our results therefore confirm that the bar and gas abundances in disk galaxies are anti-correlated, and that this anti-correlation does not seem to depend on the specific morphology of disks

D. Neutral Hydrogen Excess $\gamma_{\rm HI}$

This property is defined as

$$\gamma_{\rm HI} = \frac{f_{\rm HI} - \langle f_{\rm HI} \rangle}{\sigma_{f_{\rm HI}}} \,, \tag{3}$$

with the expected value of the HI mass fraction, calculated from the expression ([12]).

$$\langle f_{\rm HI} \rangle = -0.328 \log M_* - 1.492(g-r) + 3.662 \,, \tag{4}$$

and $\sigma_{f_{\rm HI}} = 0.272$ dex its scatter.

In this case, it is necessary to deal with a volume-limited sample which reduces the available data to a total of 1222 galaxies of which 232 present a bar. Again we have enough statistics to study the galaxy types Sa, Sb and Sc separately.

Since bars are more likely in redder spirals which have more stars and which also have less atomic gas, the skeptical astronomer could say the result in the previous Section has nothing to do with the gas content at all, just

that the types of galaxies with less bars have more gas. As the results depicted in Figure (6) demonstrate galaxies *at a given stellar mass* are less likely to be found hosting a bar if they are gas rich, so it is likely the atomic gas which is driving the correlation. Also note that the larger errors may explain why the bar fractions in the extremal bins of Figure (6) are not well aligned with morphology.

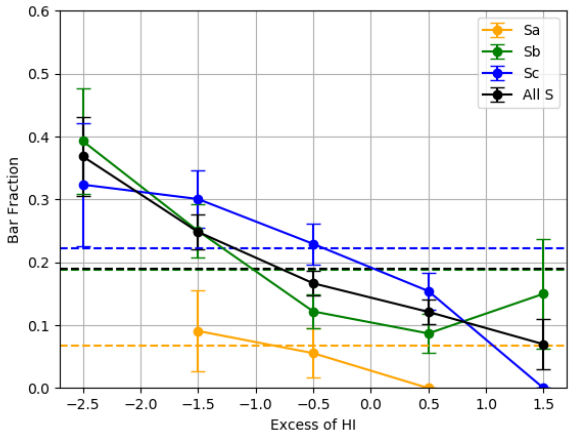

FIG. 6: Representation of the bar fraction vs the excess of HI, for the Sa (yellow), Sb (green), Sc (blue) and all the galaxy types (black). The discontinuous lines are the average value.

V. CONCLUSIONS

Using the HI content information from the Arecibo Legacy Fast ALFA survey catalog, we have studied the fraction of galaxies hosting bars as a function of their stellar and atomic gas content. We have completed the neutral gas observations with the extensive optical/NIR data gathered in the NASA-Sloan Atlas spectroscopic catalog, as well as with the information on galaxy morphologies and bar likelihoods provided in the recently published catalog by [15] that relies on automated classification algorithms.

We confirm previous results by [14], finding a bimodal behavior for the dependence of the bar probability of the disk population on both the stellar mass and the $(g - r)$ optical color. Although these authors attribute their result to a deficit of galaxies with the characteristic mass and color that define the transition from the blue cloud to the red sequence, the fact that the different subtypes of disk galaxies do not reproduce this behavior suggests that the observed bimodality could simply be due to the tendency of the late disks to be of low-mass and blue, while earlier spirals are more massive and redder.

We also find a strong negative correlation between the bar fraction and the HI content of galaxies measured either from the total neutral gas mass ratio or from the excess of atomic gas, in good agreement with [13]. This dependence is usually explained invoking two mechanisms: (i) that bars promote the consumption of atomic gas, and (ii) that gas prevents the formation/growth of bars. The fact that the galaxies with the highest relative gas content (Sc) are also the most barred disks suggests that barred objects are not consuming their gas in a more efficient way than their unbarred counterparts, hence favoring the second explanation.

Acknowledgments

I would like to thank my advisor José Maria Solanes Majua for the advice and support through the long work done, that without his guidance would have not been possible. My colleagues for their encouragement and always being there, and finally my family for their unconditional support, patience and love that has helped me over these years.

[1] Athanassoula E., 2003, MNRAS, 341, 1179
[2] Cheung E., et al., 2015, MNRAS, 447, 506
[3] Ostriker J.P., Peebles P.J.E., 1973, ApJ, 186, 467
[4] Sellwood J.A., 2014, Reviews of Modern Physics, 86, 1
[5] Sheth K., et al., 2012, ApJ, 758, 136
[6] Abazajian, K.N. et al., 2009, ApJS, 182, 543
[7] Haynes, M.P. et al., 2018, ApJ, 861, 49
[8] Willett, K.W., et al., 2013, MNRAS, 435, 2835
[9] de Vaucouleurs, G., 1977, Proc. of a Conference at Yale University, eds. B.M. Tinsley & R.B. Larson. (New Haven: Yale Univ. Obs.), p. 43
[10] Haynes, M.P., & Giovanelli, R. 1984, AJ, 89, 758
[11] Baldry, I.K., et al. 2004, ApJ, 600, 681
[12] Zu, Y., 2018, eprint arXiv:1808.10501
[13] Masters, K.L., et al. 2012, MNRAS, 424, 218
[14] Nair, P.B., & Abraham, R.G. 2010, ApJL, 714, L260.
[15] Domínguez Sánchez, H., et al. 2018, MNRAS, 476, 3661
[16] Giovanelli, R., et al. 2005, AJ, 130, 2598
[17] Boselli, A. et al. 2011, A&A, 528, 107
[18] Toribio, M.C., et al. 2011, ApJ, 732, 93
[19] The ALFALFA survey is not exactly flux limited given that the probability of detection also depends on the observed width of the 21-cm line.